

RSC Advances



This is an *Accepted Manuscript*, which has been through the Royal Society of Chemistry peer review process and has been accepted for publication.

Accepted Manuscripts are published online shortly after acceptance, before technical editing, formatting and proof reading. Using this free service, authors can make their results available to the community, in citable form, before we publish the edited article. This *Accepted Manuscript* will be replaced by the edited, formatted and paginated article as soon as this is available.

You can find more information about *Accepted Manuscripts* in the [Information for Authors](#).

Please note that technical editing may introduce minor changes to the text and/or graphics, which may alter content. The journal's standard [Terms & Conditions](#) and the [Ethical guidelines](#) still apply. In no event shall the Royal Society of Chemistry be held responsible for any errors or omissions in this *Accepted Manuscript* or any consequences arising from the use of any information it contains.

Immobilization of papain on nanoporous silica†

Jia He^{a‡}, Ming Wu^{b‡}, Xizeng Feng^{b*}, Xueguang Shao^a, Wensheng Cai^{a*}

^a Collaborative Innovation Center of Chemical Science and Engineering (Tianjin), State Key Laboratory of Medicinal Chemical Biology (Nankai University), Research Center for Analytical Sciences, College of Chemistry, Nankai University, Tianjin, 300071, P. R. China. E-mail: wscai@nankai.edu.cn

^b State Key Laboratory of Medicinal Chemical Biology, College of Life Science, Nankai University, Tianjin, 300071, P. R. China. E-mail: xzfeng@nankai.edu.cn

† Electronic supplementary information (ESI) available.

‡ These authors contributed equally.

Abstract: Immobilization of enzymes has attracted much attention in nanoscience and nanotechnology. However, the mechanisms of recognition and immobilization are still poorly understood at atomic resolution. In this study, we report that a newly synthesized single-crystal-like, nanoporous silica particle possesses a high adsorption capacity for the immobilization of papain. The immobilized enzyme could be used in the degradation of proteins, such as bull serum albumin. Moreover, the adsorption mechanism of papain on the silica surface was investigated employing docking, classical atomistic molecular dynamics simulations and molecular mechanics Poisson-Boltzmann surface area calculations. Ten independent simulations starting from two representative initial orientations of papain toward the solid surface were performed, resulting in four representative adsorption modes. The calculated relative binding free energies of the four different modes show that the one with the binding patch primarily consisting of α -helix (ASP108~TYR116), β -sheet (GLN73, ALA76, GLN77), and turn (ARG59) is most energetically favored. Further analysis of the most favored immobilization mode demonstrates that, after initial binding to the silica, the papain optimized its conformation to allow more atoms to contact with the surface. Electrostatic and van-der-Waals interactions drove in a cooperative fashion for the adsorption, wherein van-der-Waals contributions are the primary component of the binding free energy in most energetically favored adsorption mode. Besides, the global structure of the papain was preserved in the course of adsorption. Slight structural rearrangements at the entrance of the active site were observed, which increase the accessibility of the active site to solvent and presumably to substrates, and thus could facilitate productive binding between substrates and papain.

Keywords: papain, nanoporous silica particles, enzyme immobilization, molecular dynamic simulation, molecular mechanics Poisson-Boltzmann surface area calculation

1. Introduction

Enzymes are important and indispensable processing aids in agrochemicals, pharmaceuticals, and fine chemicals.¹⁻⁴ Yet the application of most enzymes, including protease, is quite limited due to instability, poor recovery, and low reusability. Immobilization has long been recognized as a useful method for retaining enzymes in bioreactors, enabling the continuous processes, and improving the adaptability to various engineering designs.⁵⁻⁹ Recently, several new types of nanomaterial, such as nanoporous supports and nanoparticles,¹⁰⁻¹⁴ are widely implemented to improve traditional immobilized enzyme performance.

However, the potential functional capacity of immobilized enzymes, without a detailed structural understanding of immobilization process and mechanism, is not predictable. In the biological and biomedical applications, much work is ongoing to characterize the interactions of protein with nanomaterial by spectroscopy and chromatography methods.¹⁵⁻¹⁶ Nevertheless, atomic-detail insights into enzyme-nanomaterial complexes are still difficult to obtain through conventional methods because of the high surface-to-volume ratio of nanomaterial.^{15,17-18} Many technologies are emerging that will enable a better understanding of the bio-nano interface. Among these methods, theoretical explorations have proven to be a powerful tool that can effectively complement experimental studies of protein-nanomaterial and peptide-surface systems.¹⁹⁻³⁰

Papain, a sulfhydryc protease extracted from the latex of *Carica Papaya*, is a prime example of the family of cysteinic proteins. As a cysteinic protease with a thiol group at its active site, it is an excellent structural model for this group of enzymes known to participate in the degeneration of proteins.³¹ Silica materials with defined structures and surface properties are often used in the area of catalysis, sorption, drug delivery, etc.³²⁻³⁴ Recently, the adsorption of papain on silica nanomaterial has been drawing much attention.³⁵⁻³⁸ On the basis of the experimental data, it was concluded that papain could be adsorbed on silica nanomaterial. Herein, we report that a newly synthesized single-crystal-like, nanoporous silica particle,³⁹ Santa Barbara

Amorphous material-1 (SBA-1), could efficiently immobilize papain using sodium dodecyl sulfate polyacrylamide gel electro-phoresis (SDS-PAGE). To assess the catalytic properties of the enzyme, the papain immobilized on this carrier has been applied in the hydrolysis of protein.

In order to unveil the preferred immobilization mode, structural details and adsorption dynamics on the large nanopores of the particles, which could be approximated as a plane compared to the length scale of the enzyme, we present the investigation on the interactions of papain and silica surface, employing molecular docking, molecular dynamics (MD) simulations, and molecular mechanics Poisson-Boltzmann surface area (MM-PBSA) calculations. The results of simulations shed insights into the papain-silica interactions, and may further explain our experimental observation. The present work highlights the mechanism and application of immobilization of enzymes on nanomaterials.

2. Experimental

2.1 Protein adsorption experiments

Papain was dissolved by phosphate-cysteine Disodium ethylenediaminetetraacetate buffer (pH 6.0) to make enzyme solutions with the concentration of 5 mg ml⁻¹. The SBA-1³⁹ was generously provided by Prof. Tie-Hong Chen in College of Chemistry, Nankai University, Tianjin, China. It has two groups of pores; one has the diameter of 3 nm, the other ranging from 10 to 50 nm. As a reference, a kind of silica sphere with uniform pore size (pore diameter is 2 nm), Mesoporous Crystalline Material-41 (MCM-41), was also prepared. In each adsorption experiment, the same amount of SBA-1 and MCM-41 (5 mg) was suspended in 1 ml 5 mg ml⁻¹ papain solution. The resulting mixture was continuously shaken for 2 h at 120 rpm at room temperature. The equilibrated samples were centrifuged for 5 min at 5000 rpm. The supernatant liquid was transferred to a new centrifuge tube. Each precipitate was resuspended with phosphate-cysteine Disodium ethylenediaminetetraacetate buffer (pH 6.0) and then centrifuged for 5 min at 5000 rpm. Repeat for three

times and then each sample supernatant liquid was put together. The amount of papain adsorbed was calculated by subtracting the amount found in the supernatant liquid and eluent after adsorption from the amount of papain present before addition of the SBA-1 or MCM-41.

2.2 Assessment of the digestion capacity of papain on bovine serum albumin by sodium dodecyl sulfate polyacrylamide gel electro-phoresis

Electrophoresis of proteins was performed using regular SDS-PAGE (Bio-Rad, Hercules, CA) with 15% separating and 5% stacking gels. Proteins were stained with Coomassie Brilliant Blue R-250. As soon as adsorption finished, the two spheres were centrifuged at speed of 5000 rpm for 5 min. 10 μl of the supernatant was added to the gel (lane 4 and 5) and the sediment was washed three times with phosphate-cysteine Disodium ethylenediaminetetraacetate buffer (pH 6.0). Washed spheres were resuspended in 500 μl phosphate-cysteine disodium ethylenediaminetetraacetate buffer, sonicated and then took out different volume (50 and 150 μl), adding to 100 μl bovine serum albumin (BSA, 4 mg ml^{-1}), and adjusting total volume of each group to 250 μl with phosphate-cysteine disodium ethylenediaminetetraacetate buffer and incubated at 60 $^{\circ}\text{C}$ for 10 min while shaken at 120 rpm.

2.3 Molecular dynamics simulations

2.3.1 Molecular models. The initial coordinates of papain with 212 amino acids was taken from the crystal structure solved at 1.65 \AA resolution (PDB code: 9PAP). The oxidized Cys25 side chain was “reduced” to $-\text{SH}$ to regenerate the native protein.⁴⁰⁻⁴⁷ The residue His159 was fully protonated owing to the study of Shokhen.⁴³ All other titratable protein side chains were assigned their standard protonation state with PROPKA⁴⁸⁻⁵¹ at pH 6.0, consistent with the experimental conditions. Meanwhile, three disulfide bonds in the crystal structure were retained. Subsequently, the molecular model was sufficiently relaxed in an

explicit water environment by an equilibrium simulation of 10 ns. The root-mean-square deviation (RMSD) values of the papain fluctuate around 1.6 Å as a function of time (see the ESI), suggesting that the whole protein is stable in the aqueous medium. The equilibrium structure of papain was applied as an initial conformation for the docking and MD simulation of protein adsorption.

Modeling of the mesoporous silica surface is a rather complicated question. For the small pore of mesoporous silica (diameter < 3 nm), the curved silica surface model was more frequently used to explore the adsorption properties of small molecules.⁵²⁻⁵⁴ The pore diameter of MCM-41 is 2 nm. The SBA-1 used in this study has two types of pores, 3 nm and 10-50 nm.³⁹ The experimental results demonstrated that papain was mainly adsorbed on the outer surface and the large pores of the nanoporous silica. It is difficult for this protein (3-5 nm) to enter into the small pores (diameter < 5 nm) on account of steric hindrances. Thus, the primary purpose of the computations is to investigate the adsorption behavior of papain on the outer surface and the large pores surface of the SBA-1 particle. Compared to the length scale of the papain, the curvature of the surfaces of the particles and the large pores can be ignored. On the other hand, both crystalline silica and amorphous silica could be used to model the silica surface.⁵²⁻⁵⁴ Therefore, the model of even crystalline silica surface was employed in this study.

Quartz is the most common form of crystalline silica. Among the various crystal surfaces, Q³, i.e., a chemical environment of (Si-O)₃Si(-OH) for superficial Si atoms with one silanol, is more common than other environments in silica matrix.²⁷ The Q³ surfaces (see the ESI) were prepared from the [1 0 -1] cleavage plane of α -cristobalite and hydrated to form silanol groups, and match the typical area density of 4.7 silanol groups per nm² surface area reported in experimental studies.⁵⁵⁻⁵⁶ In a thermally unprocessed Q³ silica surface, only about 5.9% of silanol groups are deprotonated at pH 6.0,²⁸ which might be partly affected by the synthetic origin and on the total ionic strength in solution. In this model, we approximated the ratio by 0%, and the silica surface was fully capped with OH groups.

2.3.2 Papain-silica systems. The adsorption of papain on the silica surface depends on the initial orientation relative to the surface. The papain is prevented from significant rotational and translational motions on the time scale of nanoseconds. To overcome this limitation, we used the PatchDock⁵⁷⁻⁵⁸ package to perform docking calculations and the predicted complexes were further refined by the FireDock⁵⁹⁻⁶⁰ program to determine the most favorable initial orientations for the papain on the silica surface. The representative structures of the top two computed complexes ranked by the highest docking scores were selected as representative starting configurations (see the ESI). To avoid the papain from being in a kinetically trapped state where only minor relaxation could take place, the nearest distance between the papain and the silica surface was set to 8 Å, retaining the original docked orientation with respect to the surface (see Figure 1). A cubic simulation box of dimension (103 Å × 103 Å × 100 Å) including water molecules, the papain, and the silica surface was built. Chloride ions were added to achieve electroneutrality. The general description of the molecular systems considered in this study is summarized in the ESI.

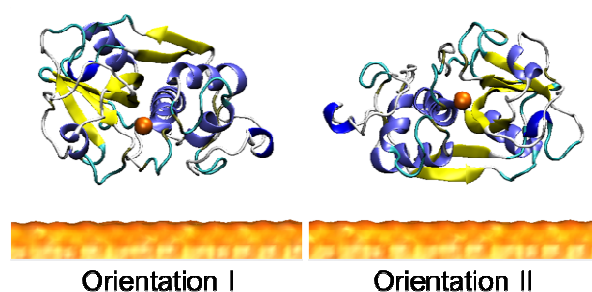


Figure 1. Two representative orientations used for adsorption simulations. Papain is represented by the new cartoon style. The atom S of residue CYS25 in active center is highlighted by orange sphere. For clarity, water molecules and ions are removed.

2.3.3 Simulation protocol. All MD simulations herein were performed with the NAMD 2.8 package.⁶¹ The CHARMM27⁶² force field was employed for the papain, and the TIP3P⁶³ water model was applied. The

parameters and atomic partial charges of silica were taken from the literature⁶⁴ and shown in Table S1. The constant temperature and the pressure were maintained at 300 K and 1 atm, respectively, using Langevin dynamics and the Langevin piston method.⁶⁵ To keep the solid surface, the pressure fluctuation was allowed only in the direction of the normal axis of the silica surface. Chemical bonds involving hydrogen atoms were constrained to their experimental lengths by means of the Shake/Rattle algorithms.⁶⁶⁻⁶⁷ Periodic boundary conditions (PBCs) were applied in the three directions of Cartesian space. A 14-Å cutoff was introduced to truncate van-der-Waals interactions. Long-range electrostatic forces were taken into account by means of the particle mesh Ewald (PME) algorithm.⁶⁸ The r-RESPA multiple time-step algorithm was employed to integrate the equations of motion with a time step 2 and 4 fs for short- and long-range interactions, respectively.⁶⁹ Visualization and analysis of the MD trajectories were performed with the VMD package.⁷⁰ Each solvated system before production simulation underwent 5000 steps of energy minimization, 10 ps of heating from 0 to 300 K, and then 400 ps of water equilibration. To reproduce the experimental dielectric constant of silica substrate, a restraint file with constants of 20.0 kcal mol⁻¹ Å⁻² enforced on Si atoms and inner O atoms was employed, which have been found to be optimal by the previous research.⁷¹ The isolated and vicinal silanol groups of silica surface and the enzyme papain were free to move during the production run. A non-covalent approach was chosen to study the interaction between enzyme and solid surface. Five independent simulations were performed for each initial orientation.

2.4 Molecular mechanics Poisson-Boltzmann surface area calculation

Prediction of binding free energies describing protein and solid surface adsorption from the MD simulations remains a daunting computational endeavor. In the recent years, MM/PBSA combined with the MD simulations has been considered as a fast and effective method to calculate binding free energy. MM/PBSA is already implemented, optimized and validated in the NAMD package.⁷² In the present work,

the MM-PBSA method was employed to compare the relative binding affinities of papain and silica among different adsorption modes. The binding free-energy was based on “snapshot” configurations taken every 100 ps from the last 10 ns of the MD trajectories. All water molecules were removed for the different sized systems.

The free-energy of each complex is given by the equation:

$$G = E_{MM} + G_{PB} + G_{NP} - TS \quad (1)$$

where E_{MM} is the molecular mechanics energy of the solute in the gas phase, composed of the bond, angle, torsion, van-der-Waals and electrostatic terms. G_{PB} and G_{NP} are the electrostatic and hydrophobic parts of the solvation free-energy. The last term in equation 1 is the solute entropy. The binding free-energy can be obtained by:

$$\Delta G = G_{\text{complex}} - G_{\text{papain}} - G_{\text{silica}} \quad (2)$$

The focus in this work is the binding free-energy difference between different adsorption modes. The free-energies of papain and silica are the same for all the molecular systems. The entropic terms, which are much smaller than the other terms.⁷³ We suppose that the entropic contributions for the different adsorption modes are similar. Therefore, the entropic contributions to the relative binding affinity are not considered in the present work. Therefore, the binding free-energy difference is given by:

$$\Delta\Delta G = (\Delta E_{MM} + \Delta G_{PB} + \Delta G_{NP})_{\text{complex}} \quad (3)$$

The MM-PBSA analysis was performed using the same force field employed in the MD simulations for the MM contribution and APBS⁷⁴ for the Poisson–Boltzmann contribution. For the APBS calculation, the iAPBS⁷² interface was used to call APBS from NAMD. In the iAPBS interface from NAMD, the non-polar solvation term G_{NP} in Equation 3 is approximated by a linear function of the solvent-accessible surface area:

$$G_{NP} = \gamma * \text{SASA} \quad (4)$$

where γ is the surface tension for apolar energies. The surface tension was set to 0.105 kcal mol⁻¹ Å⁻² in the

calculation of G_{NP} . Thereinto, the protein dielectric was set to 1.0, the solvent dielectric was set to 80.0, the solvent radius was set to 1.4 Å, the grid spacing was 0.5 Å in each dimension, and the rest of the parameters were default values.

3. Results and discussion

3.1 Immobilized papain on SBA-1 for BSA hydrolysis

For nanoporous particles, besides adsorption on the outer surface of the particles, proteins can adhere to the surface of the pores that are larger than their hydraulic radius. The length scale of the papain is 3-5 nm, much smaller than the large pore size of the SBA-1 particle. Thus, the papain molecules may also adsorb into the large pores of the SBA-1 particle. It is difficult, however, for this protein to enter into the pores of MCM-41 on account of steric hindrances.

We compared the absorbing capacity of SBA-1 and MCM-41 by the SDS-PAGE method. As shown in Figure 2, a stronger papain band intensity was observed in lane 4, compared to lane 3. This demonstrated that SBA-1 has a higher adsorption capacity for papain than MCM-41. Similarly, a weaker BSA band intensity was observed in lane 5, compared to lane 7, indicating that the amount of papain adsorbed by SBA-1 is much larger than that of MCM-41. The same conclusion can also be reached by comparing lane 6 with 8.

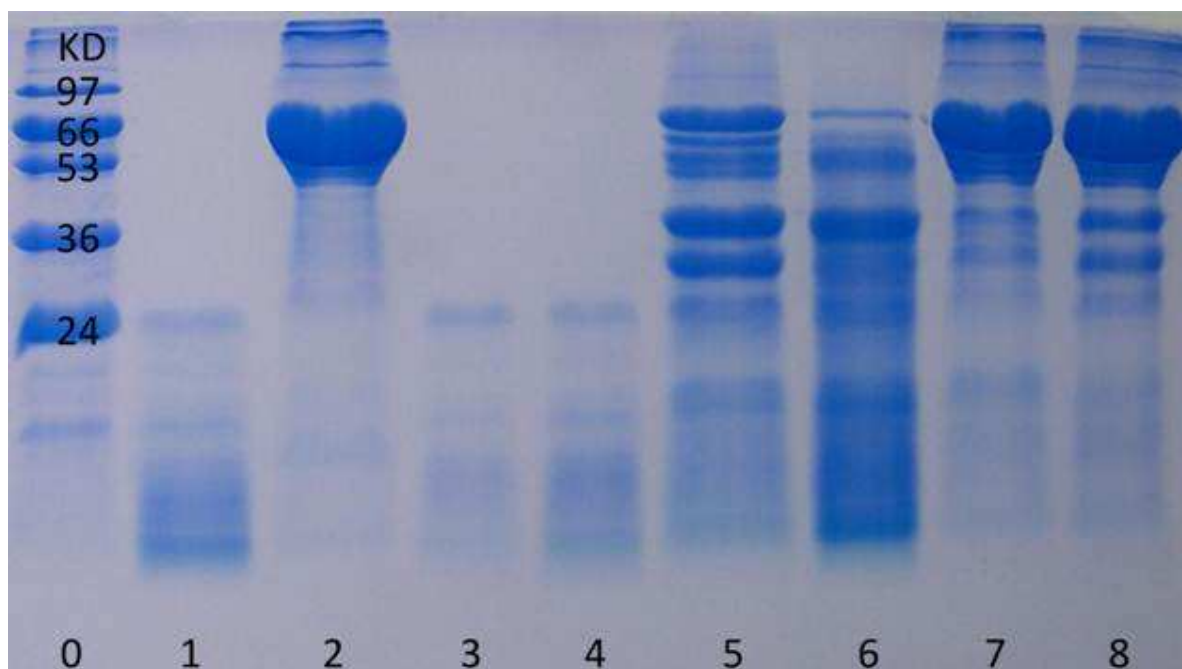


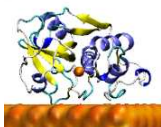
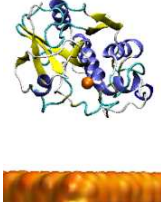
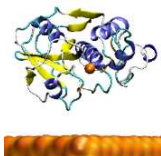
Figure 2. SDS-PAGE patterns of BSA digested by SBA-1 fully loaded with papain. Proteins were separated by electrophoresis on a 15% SDS-polyacrylamide gel. The material in each well was as follows: lane 0, protein molecular weight marker; Lane 1, 5 mg ml^{-1} papain; lane 2, 4 mg ml^{-1} BSA; lane 3: supernatant of first time centrifugation papain and SBA-1 complexes solution. Lane 4: supernatant of first time centrifugation papain and MCM-41 complexes solution. Lane 5-6, SBA-1-papain complexes: BSA (w/w) was 1:2, 1.5:1, lane7-8, MCM-41-papain complexes: BSA (w/w) was 1:2, 1.5:1.

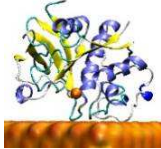
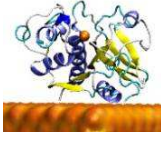
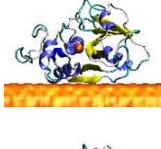
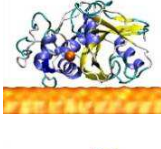
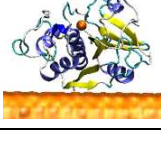
Electrophoresis of proteins was performed using regular SDS-PAGE (Bio-Rad, Hercules, CA) with 15% separating and 5% stacking gels. $10 \mu\text{l}$ of samples were added into 5% stacking gels for 10 min at 80 V, then change the voltage to 120 V for another 1 h. A wide range molecular weight marker (Sigma) was included in each gel. Proteins were stained with Coomassie Brilliant Blue R-250. The experiment is based on the premise that papain can degrade BSA and the digestion effect was concentration dependent (see the ESI).

3.2 Immobilization modes

The results of ten independent MD runs for two orientations with different initial velocities are gathered in Table 1. In eight out of the ten runs, adsorption of the papain on the silica surface was observed, whereas it does not occur in the other two runs. Only the eight adsorption cases were further discussed. The evolution of the RMSD of the papain with respect to its initial structure was monitored as a function of time (see the ESI). It increases in the initial stage and reaches a plateau in the last 10 ns, indicating that after reorganization, the papain becomes stable. The last 10-ns trajectories are, therefore, used for further analysis. Through statistical analysis of the adsorbed residues over the eight 10-ns trajectories, four stable immobilization modes could be discerned according to different adsorption patches, labeled as mode A, B, C and D respectively. Orientation I-n1, n2 and orientation II-n1, n2 are chosen as representative structures for each adsorption mode and shown in Figure 3.

Table 1 Orientations of the papain on the silica surface obtained by the MD simulations

System	Time (ns)	Final orientation	
Orientation I-n1	30	Mode A	
Orientation I-n2	30	Mode B	
Orientation I-n3	40	Non-adsorption	
Orientation I-n4	40	Non-adsorption	

Orientation I-n5	30	Mode B	
Orientation II-n1	30	Mode C	
Orientation II-n2	40	Mode D	
Orientation II-n3	30	Mode D	
Orientation II-n4	30	Mode D	
Orientation II-n5	30	Mode C	

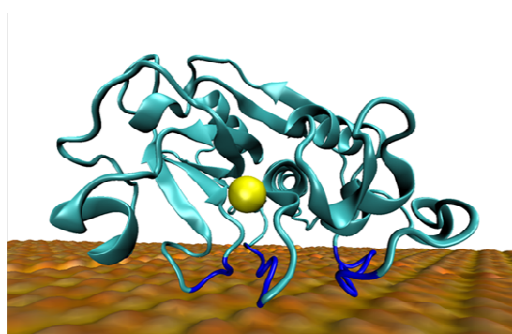
Mode A. The global orientation of the protein with respect to the surface was maintained as its initial orientation. The flexible turn and coil of the papain bind the surface via residues LYS17~SER21, ASN84~VAL91, GLY178~GLY180. No residues of the C-terminal or N-terminal tail were found to directly contact the silica surface.

Mode B. The global orientation of the papain in this mode has been rotated during adsorption, as visible from the MD trajectory. The binding of the papain to the surface is stabilized by a strong reorganization of α -helix via LEU143, ARG145, and strengthened by turn via SER21. The C-terminal or N-terminal end does not adsorb on the surface of silica.

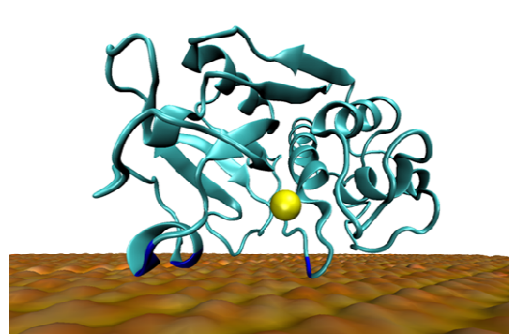
Mode C. From the trajectory, the C-terminus (ASN212) and N-terminus (ILE1) of papain were observed to firstly anchor on the silica surface, inducing a global rotation of the protein with respect to the surface.

Then, the enzyme adjusted its orientation and adsorbed on the surface through residue GLN114 and ALA120. In the adsorbed complex, the α -helical segment (GLN118~ASN127) and the β -sheet (GLY109~VAL113) segment were nearly parallel to the silica surface.

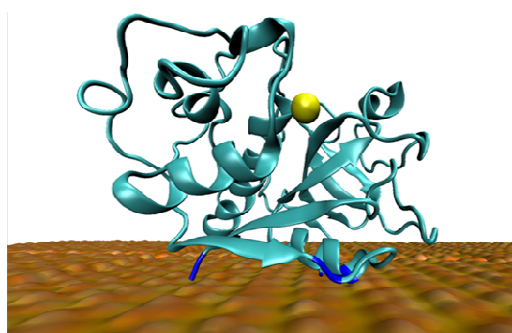
Mode D. The MD trajectory showed that the C-terminal tail (ASN212) firstly anchored on the silica surface. The N-terminal tail turned away from the surface and allowed the protein bind through the patch of the α -helix (ASP108~TYR116), β -sheet (GLN73, ALA76, GLN77), and turn (ARG59). The adsorption was accompanied by a slight unfolding of the α -helix, which could be ascribed to the interaction with the surface.



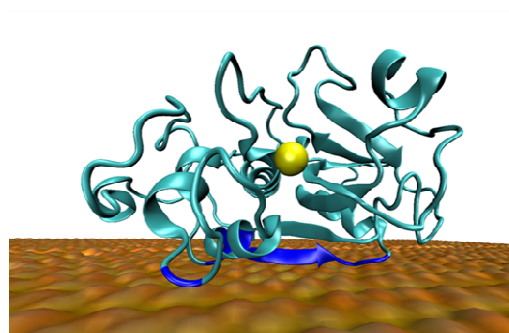
Mode A – 16 adsorbed residues: LYS17~SER21, ASN84~VAL91, GLY178~GLY180



Mode B – 3 adsorbed residues: SER21, LEU143, ARG145



Mode C – 4 adsorbed residues: ILE1, GLN114, ALA120, ASN212



Mode D – 13 adsorbed residues: ARG59, GLN73, ALA76, GLN77, ASP108~TYR116

Figure 3. Side view of the papain after adsorption. Eight adsorbed structures are clustered into four classes, mode A, B, C, and D. Orientation I-n1, n2 and orientation II-n1, n2 are chosen as representative structures for each adsorption mode. Papain is represented by the new cartoon style, and the adsorbed residues are colored in blue. The atom S of residue CYS25 in active center is highlighted by yellow sphere. The adsorbed

residues are defined as the residues with their centroids within 6 Å around the solid surface and their residence time on the surface was more than 9 ns in the last 10 ns trajectory.

In order to investigate the optimal immobilization mode, the relative binding free energies between the papain and the silica surface were calculated by means of the MM-PBSA method based on the last 10 ns MD trajectories, and the results are displayed in Table 2. The entropy contributions of the water molecules in the solvation shell and the protein itself are ignored due to the slightly alterations in the main structure of the papain (see below). It is apparent that mode A and D are energetically favored. It was mainly contributed by the molecular mechanics energy of papain and silica including van der Waals and electrostatic interaction, on account of possessing more adsorbed residues. By further comparing mode A and D, the contributions of ΔE_{MM} and ΔG_{NP} terms are almost identical. The major difference of the binding free energies results from the ΔG_{PB} term. In mode D, 31% of the adsorbed residues, compared to only 13% in mode A, are hydrophobic, giving rise to the favorable desolvation energy. Therefore, mode D is most energetically favored and stable.

Table 2 Summary of MM-PBSA results^a

System	ΔE_{MM}	ΔG_{PB}	ΔG_{NP}	$\Delta\Delta G$
Mode A	-127	56	-27	-98
Mode B	-5	-16	3	-18
Mode C ^b	0	0	0	0
Mode D	-127	47	-29	-109

^aAll results are in kcal mol⁻¹.

^bMode C is defined as a reference state.

3.3 Conformational changes

The overall size of the protein was monitored in each immobilization mode by calculating the radius of

gyration (R_g) (see Table 3). There was no obvious expansion of the size of papain after the adsorption in all cases. Besides, the small root-mean-square fluctuation (RMSF) value of each residue showed that the main structure of the papain was preserved in the course of adsorption (see Figure 4). It can be attributed to the three strong disulfide bonds. The overall shape of papain is characterized by the eccentricity (see Table 3). The eccentricity is defined as $1 - I_{\text{ave}}/I_{\text{max}}$, where I_{max} is the maximal principal moment of inertia and I_{ave} is the average of three principal moments of inertia. The eccentricity is zero for a perfect sphere and close to 1 for a flat or needlelike ellipsoid.¹⁹ The calculated average eccentricity of each molecular system is close to 0, indicating that the shape of the papain after adsorption is close to a sphere for different adsorption modes. Mode D is found to possess the largest eccentricity. This deformation makes the protein more compact to the solid surface.

Table 3 Summary of simulation systems with averaged papain properties^a

System	$R_g^b/\text{\AA}$	Eccentricity	$\text{SASA}_{\text{active_site}}^c/\text{\AA}^2$
Mode A	16.59 ± 0.04	0.12 ± 0.01	147.0 ± 24.5
Mode B	16.59 ± 0.04	0.09 ± 0.01	125.6 ± 11.2
Mode C	16.64 ± 0.06	0.10 ± 0.01	120.2 ± 18.4
Mode D	16.63 ± 0.05	0.16 ± 0.01	138.2 ± 24.6
Free state	16.57 ± 0.04	0.15 ± 0.01	111.4 ± 10.4

^aAll data are averaged over the last 10-ns simulations.

^b R_g : radius of gyration.

^c $\text{SASA}_{\text{active_site}}$: solvent-accessible surface area of the active site of papain. The active site is composed of residues GLN19, CYS22, GLY23, SER24, CYS25, HIS159, ASN175 and SER176.

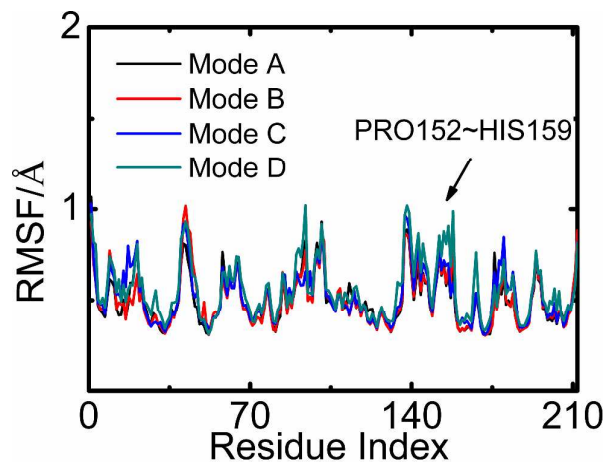


Figure 4. RMSF of backbone carbon atoms of each residue averaged over the whole MD trajectory.

Although the global structure of the papain was preserved, the immobilization process might affect the exposure of its active site to substrates, leading to a low substrate specificity and catalytic efficiency. The exposure level of the active site to the solvent is characterized by its solvent-accessible surface area (SASA). The active site includes the CYS25 and HIS159 catalytic group, as well as residues associated with them. The SASA was measured by the VMD package using a solvent probe radius of 1.4 Å. As reported in Table 3, the active site is not buried by the silica surface but more exposed in all the four cases, compared to the free state, particularly for mode A and D. Furthermore, analyzing the structural features of the active site for each molecular system shows that the five cases in Table 3 can be classified into two categories, viz. open and closed state. As shown in Figure 5, mode A and D are similar, wherein the CYS25-HIS159 catalytic diad appears to adopt an open conformation, whereas this active site is found in a closed conformation for the free state and mode B and C. The transition from the closed to the open conformation is mainly attributed to the breakage of the hydrogen bond between HIS159 and ASN175. The peaks of PRO152~HIS159 for mode D in Figure 4 indicate that these residues underwent slight structural rearrangements. Such structural rearrangements at the entrance of the active site increase its accessibility to solvent and presumably to substrates and could facilitate productive binding between substrates and enzyme. It is worth noting that the

active site might be buried and inactive with the decrease of the pore size of the nanoporous silica, although the enzyme may possess higher binding free-energy to the silica surface.

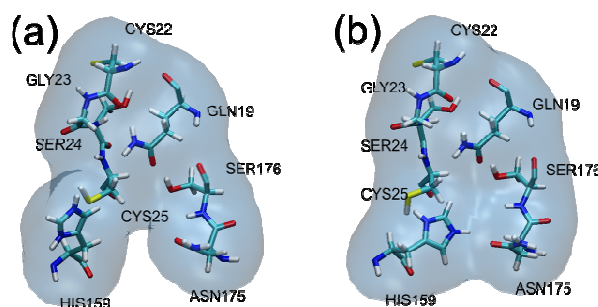


Figure 5. The active site of the papain is in an open conformation for mode A and D (a), and in a closed conformation for free papain and mode B and C (b). The complete adsorption structures of papain on the silica surface are shown in Figure 3. The distances between the center-of-mass of the active center and the silica surface for mode A, B, C and D are 8.5 Å, 9.6 Å, 24.5 Å and 16.9 Å, respectively.

3.4 Adsorption Dynamics

To understand the adsorption dynamics, the main geometrical quantity, namely the time evolution of the papain center-of-mass distance to the silica surface and the contact area between the silica surface and the protein is characterized and shown in Figure 6. The contact area is determined by the equation:

$$\text{Contact area} = ((S_{\text{protein}} + S_{\text{surface}}) - S_{\text{complex}})/2 \quad (4)$$

where S_{protein} and S_{surface} are the SASA of the isolated protein and the silica surface, respectively, and S_{complex} is that of the whole assembly of these two motifs.

For mode A, the distance/contact area decreases/increases gradually in the first 12 ns and then becomes stable, indicating that the final adsorption was achieved. For mode B, the contact area sharply increases from 0 to a certain number at 10 ns and then quickly reaches a plateau, which means adsorption occurred at 10 ns, but completed fast. The distance and contact area in mode C change in two steps. Combining the MD

trajectory, it is shown that the C-terminus and N-terminus of papain firstly anchored on the silica surface within 5 ns, forming a metastable state, and then the enzyme adjusted its structure gradually (12-16 ns) to reach the final stable state. For mode D, the contact area increases gradually after 10 ns, and levels off after ca. 20 ns. The distance, however, does not change in the same trend. After 15 ns, only a slight decrease is observed, but the contact area has kept a steady increase until 20 ns. It means that after binding to the surface, the papain was still optimizing its conformation at the interface to allow more atoms to contact with the surface. In summary, among the four modes, adsorption of mode D is found to be slowest. From the final adsorption results, however, the enzyme in mode A and D is closer and more compact to the surface, compared to in mode B and C.

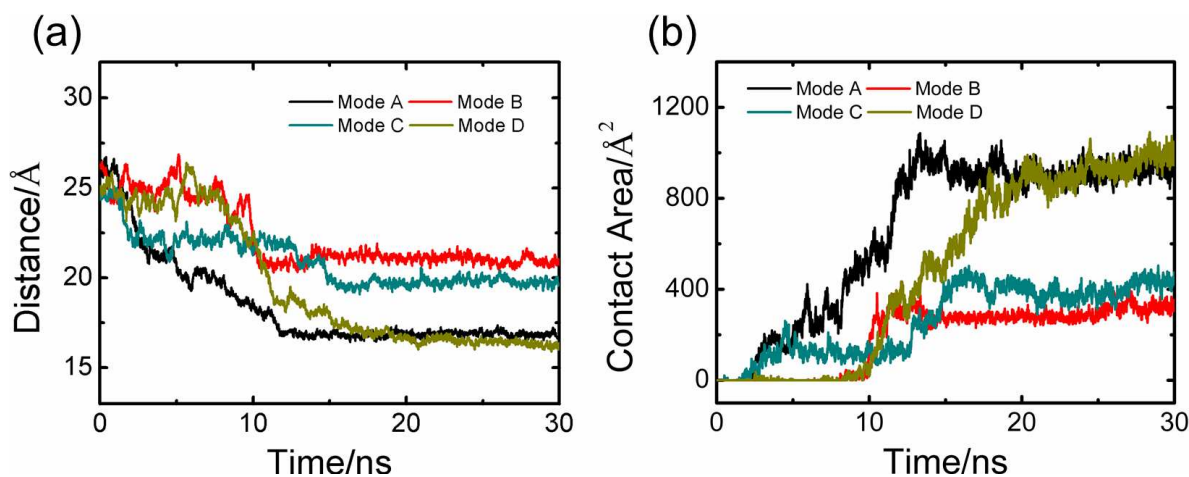


Figure 6. (a) Center-of-mass distance between the papain and the silica surface as a function of simulation time. (b) Evolution of the contact area between the papain and the silica surface.

The energetics of adsorption is displayed in Figure 7, including van-der-Waals, electrostatic interactions and total interaction energy of the papain and the silica surface. For each mode, the initial adsorption is reflected by a corresponding steady decay of the energies, and the latter level off in the final stage, indicative

of a convergence of the adsorption simulations. For mode C, the decrease of interaction energies undergoes two steps, which is consistent with the changes of the distance and the contact area. The interaction energy for mode D decreases to a constant value in a longer simulation time, compared to mode A-C. This is the reason that additional 10 ns MD simulation was performed for mode D. From the evolution of energy in Figure 7, it can be seen that electrostatic and van-der-Waals interactions drove in a cooperative fashion for the adsorption, wherein van-der-Waals contributions are the primary component of the binding free energy for mode A and mode D. Moreover, the total interaction energies for mode A and D are considerably stronger than the other two modes, in agreement with the relative ΔE_{MM} in Table 2.

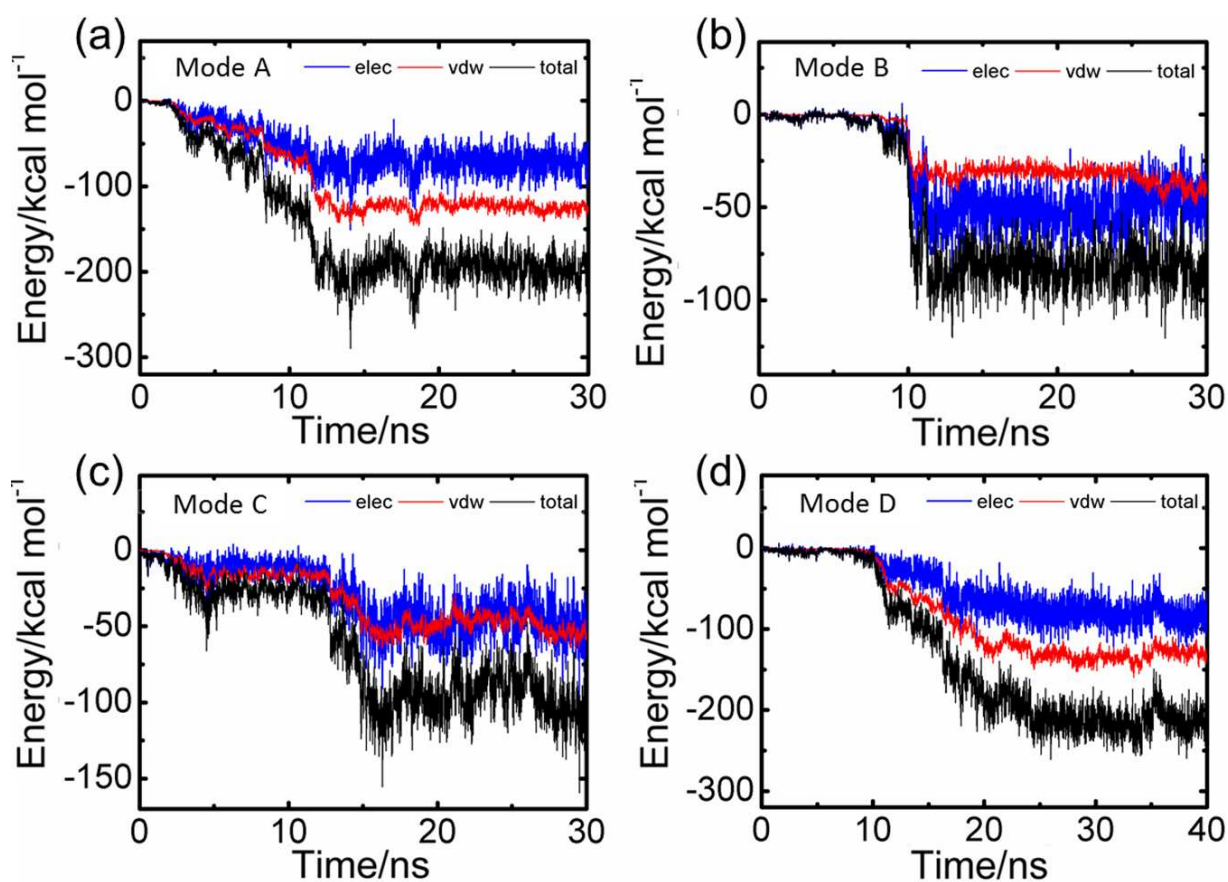


Figure 7. Energy characterizing the interaction of the papain and the silica surface.

4. Conclusion

We have presented a comprehensive computational and experimental study on the interaction of papain and a silica particle employing docking, classical atomistic MD simulations, MM-PBSA calculations and the SDS-PAGE method. SBA-1 was proven to have a higher adsorption capacity for papain than the control nanoporous sphere. The papain immobilized on this carrier could be used in digestion of BSA. On the basis of the docking and MD simulation results, four possible immobilization modes have been selected for further investigation. To determine the most stable adsorption mode, the binding free energies for different adsorption conformations were calculated. The results show that, for the most energetically favored adsorption mode, the binding site of papain is primarily located in its patch consist of α -helix (ASP108~TYR116), β -sheet (GLN73, ALA76, GLN77), and turn (ARG59). In the most favorable adsorption mode, the main secondary structures were preserved in the course of adsorption. Moreover, the active center of papain is exposed to solvent, which facilitates the subsequent hydrolysis with protein. It has been shown that van-der-Waals and electrostatic interactions constitute the main driving forces responsible for the immobilization. The results and analysis presented here contribute to improve our understanding of the immobilization process at the atomic level.

Acknowledgements. This study is supported by National Natural Science Foundation of China (No. 21373117) and Natural Science Foundation of Tianjin, China (No. 13JCYBJC18800).

Electronic supplementary information (ESI) available: Detailed information of the molecular systems, conformations of the top two docked complexes, analysis of the MD trajectories, and digestive pattern of different concentrations of BSA digested by the immobilized papain are provided.

References

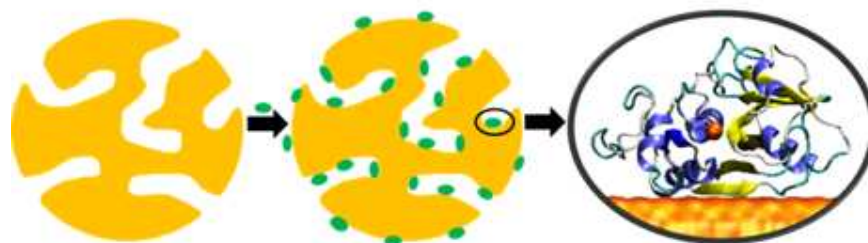
- 1 M. Vellard, *Curr. Opin. Biotech.*, 2003, **14**, 444-450.
- 2 O. Kirk, T. V. Borchert and C. C. Fuglsang, *Curr. Opin. Biotech.*, 2002, **13**, 345-351.
- 3 D. B. Sarney and E. N. Vulfsen, *Trends Biotechnol.*, 1995, **13**, 164-172.
- 4 F. Shahidi and Y. V. A. J. Kamil, *Trends Food Sci. Tech.*, 2001, **12**, 435-464.
- 5 C. Mateo, J. M. Palomo, G. Fernandez-Lorente, J. M. Guisan and R. Fernandez-Lafuente, *Enzyme Microb. Tech.*, 2007, **40**, 1451-1463.
- 6 R. A. Sheldon, *Adv. Synth. Catal.*, 2007, **349**, 1289-1307.
- 7 C. Garcia-Galan, A. Berenguer-Murcia, R. Fernandez-Lafuente and R. C. Rodrigues, *Adv. Synth. Catal.*, 2011, **353**, 2885-2904.
- 8 R. C. Rodrigues, A. Berenguer-Murcia and R. Fernandez-Lafuente, *Adv. Synth. Catal.*, 2011, **353**, 2216-2238.
- 9 J. F. Liang, Y. T. Li and V. C. Yang, *J. Pharm. Sci.*, 2000, **89**, 979-990.
- 10 J. Lei, J. Fan, C. Z. Yu, L. Y. Zhang, S. Y. Jiang, B. Tu and D. Y. Zhao, *Micropor. Mesopor. Mat.*, 2004, **73**, 121-128.
- 11 S. A. Ansari and Q. Husain, *Biotechnol. Adv.*, 2012, **30**, 512-523.
- 12 C. Ispas, I. Sokolov and S. Andreescu, *Anal. Bioanal. Chem.*, 2009, **393**, 543-554.
- 13 M. Cao, Z. H. Li, J. L. Wang, W. P. Ge, T. L. Yue, R. H. Li, V. L. Colvin and W. W. Yu, *Trends Food Sci. Tech.*, 2012, **27**, 47-56.
- 14 H. Ai, S. A. Jones and Y. M. Lvov, *Cell Biochem. Biophys.*, 2003, **39**, 23-43.
- 15 M. Mahmoudi, I. Lynch, M. R. Ejtehadi, M. P. Monopoli, F. B. Bombelli and S. Laurent, *Chem. Rev.*, 2011, **111**, 5610-5637.
- 16 S. H. D. P. Lacerda, J. J. Park, C. Meuse, D. Pristiniski, M. L. Becher, A. Karim and J. F. Douglas, *ACS Nano*, 2010, **4**, 365-379.
- 17 G. Goobes, R. Goobes, O. Schueler-Furman, D. Baker, P. S. Stayton and G. P. Drobny, *Proc. Natl. Acad. Sci. U.S.A.*, 2006, **103**, 16083-16088.
- 18 J. J. Gray, *Curr. Opin. Struct. Biol.*, 2004, **14**, 110-115.
- 19 Y. Z. Liu, M. Wu, X. Z. Feng, X. G. Shao and W. S. Cai, *J. Phys. Chem. B*, 2012, **116**, 12227-12234.
- 20 S. W. Hung, P. Y. Hsiao, M. C. Lu and C. C. Chieng, *J. Phys. Chem. B*, 2012, **116**, 12661-12668.
- 21 G. Brancolini, D. B. Kokh, L. Calzolari, R. C. Wade and S. Corni, *ACS Nano*, 2012, **6**, 9863-9878.
- 22 M. Hoefling, F. Lori, S. Corni and K. E. Gottschalk, *Langmuir*, 2010, **26**, 8347-8351.

- 23 C. Mucksch and H. M. Urbassek, *Langmuir*, 2011, **27**, 12938-12943.
- 24 T. Wei, M. A. Carignano and I. Szleifer, *J. Phys. Chem. B*, 2012, **116**, 10189-10194.
- 25 J. Schneider and L. C. Ciacchi, *J. Am. Chem. Soc.*, 2012, **134**, 2407-2413.
- 26 J. Yu, M. L. Becher and G. A. Carri, *Langmuir*, 2012, **28**, 1408-1417.
- 27 S. V. Patwardhan, F. S. Emami, R. J. Berry, S. E. Jones, R. R. Naik, O. Deschaume, H. Heinz and C. C. Perry, *J. Am. Chem. Soc.*, 2012, **134**, 6244-6256.
- 28 R. Tosaka, H. Yamamoto, I. Ohdomari and T. Watanabe, *Langmuir*, 2010, **26**, 9950-9955.
- 29 E. E. Oren, R. Notman, I. W. Kim, J. S. Evans, T. R. Walsh, R. Samudrala, C. Tamerler and M. Sarikaya, *Langmuir*, 2010, **26**, 11003-11009.
- 30 R. Notman, E. E. Oren, C. Tamerler, M. Sarikaya, R. Samudrala and T. R. Walsh, *Biomacromolecules*, 2010, **11**, 3266-3274.
- 31 I. G. Kamphuis, K. H. Kalk, M. B. Swarte and J. Drenth, *J. Mol. Biol.*, 1984, **179**, 233-256.
- 32 F. Hoffmann, M. Cornelius, J. Morell and M. Froba, *Angew. Chem., Int. Ed.*, 2006, **45**, 3216-3251.
- 33 A. Sayari and S. Hamoudi, *Chem. Mater.*, 2001, **13**, 3151-3168.
- 34 I. I. Slowing, J. L. Vivero-Escoto, C. W. Wu and V. S. Y. Lin, *Adv. Drug Deliver. Rev.*, 2008, **60**, 1278-1288.
- 35 S. Solis, J. C. Martinez, J. Paniagua and M. Asomoza, *J. Sol-Gel Sci. Techn.*, 2006, **37**, 121-123.
- 36 M. F. Wang, W. Qi, Q. X. Yu, R. X. Su and Z. M. He, *Biochem. Eng. J.*, 2010, **52**, 168-174.
- 37 F. He, R. X. Zhuo, L. J. Liu and M. Y. Xu, *React. Funct. Polym.*, 2000, **45**, 29-33.
- 38 S. Solis, J. Paniagua, J. C. Martinez and M. Asomoza, *J. Sol-Gel Sci. Techn.*, 2006, **37**, 125-127.
- 39 N. Li, J. G. Wang, H. J. Zhou, P. C. Sun and T. H. Chen, *Chem. Mater.*, 2011, **23**, 4241-4249.
- 40 K. Nishiyama, *J. Appl. Phys.*, 2010, **108**, 024701.
- 41 K. Nishiyama, *J. Appl. Phys.*, 2011, **110**, 114701.
- 42 M. Costabel, D. F. Vallejo and J. R. Grigera, *Arch. Biochem. Biophys.*, 2001, **394**, 161-166.
- 43 M. Shokhen, N. Khazanov and A. Albeck, *Proteins*, 2009, **77**, 916-926.
- 44 Y. Lin and W. J. Welsh, *J. Mol. Graphics*, 1996, **14**, 62-72.
- 45 S. Y. Reddy, K. Kahn, Y. J. Zheng and T. C. Bruice, *J. Am. Chem. Soc.*, 2002, **124**, 12979-12990.
- 46 K. Nishiyama, *Chem. Phys. Lett.*, 2010, **510**, 143-146.
- 47 K. Nishiyama, *Chem. Phys. Lett.*, 2011, **501**, 513-516.
- 48 C. R. Sondergaard, M. H. M. Olsson, M. Rostkowski and J. H. Jensen, *J. Chem. Theory Comput.*, 2011, **7**, 2284-2295.

- 49 M. H. M. Olsson, C. R. Sondergaard, M. Rostkowski and J. H. Jensen, *J. Chem. Theory Comput.*, 2011, **7**, 525-537.
- 50 H. Li, A. D. Robertson and J. H. Jensen, *Proteins*, 2005, **61**, 704-721.
- 51 D. C. Bas, D. M. Rogers and J. H. Jensen, *Proteins*, 2008, **73**, 765-783.
- 52 C. Schumacher, J. Gonzalez, P. A. Wright and N. A. Seaton, *J. Phys. Chem. B*, 2006, **110**, 319-333.
- 53 K. Yamashita and H. Daiguji, *J. Phys. Chem. C*, 2013, **117**, 2084-2095.
- 54 J. Puibasset and R. J. M. Pellenq, *J. Chem. Phys.*, 2003, **118**, 5613-5622.
- 55 A. Mendez, E. Bosch, M. Roses and U. D. Neue, *J. Chromatogr. A*, 2003, **986**, 33-44.
- 56 L. T. Zhuravlev, *Colloid. Surface. A*, 2000, **173**, 1-38.
- 57 D. Schneidman-Duhovny, Y. Inbar, R. Nussinov and H. J. Wolfson, *Nucleic Acids Res.*, 2005, **33**, W363-W367.
- 58 D. Duhovny, R. Nussinov and H. J. Wolfson, *Rome, Italy, Lecture Notes in Computer Science*, 2002, **2452**, 185-200.
- 59 E. Mashlach, D. Schneidman-Duhovny, N. Andrusier, R. Nussinov and H. J. Wolfson, *Nucleic Acids Res.*, 2008, **36**, W229-W232.
- 60 N. Andrusier, R. Nussinov and H. J. Wolfson, *Proteins*, 2007, **69**, 139-159.
- 61 J. C. Phillips, R. Braun, W. Wang, J. Gumbart, E. Tajkhorshid, E. Villa, C. Chipot, R. D. Skeel, L. Kalé and K. Schulten, *J. Comput. Chem.*, 2005, **26**, 1781-1802.
- 62 A. D. MacKerell, D. Bashford, M. Bellott, R. L. Dunbrack, J. D. Evanseck, M. J. Field, S. Fischer, J. Gao, H. Guo, S. Ha, D. Joseph-McCarthy, L. Kuchnir, K. Kuczera, F. T. K. Lau, C. Mattos, S. Michnick, T. Ngo, D. T. Nguyen, B. Prodhom, W. E. Reiher, B. Roux, M. Schlenkrich, J. C. Smith, R. Stote, J. Straub, M. Watanabe, J. Wiorkiewicz-Kuczera, D. Yin and M. Karplus, *J. Phys. Chem. B*, 1998, **102**, 3586-3616.
- 63 W. L. Jorgensen, J. Chandrasekhar, J. D. Madura, R. W. Impey and M. L. Klein, *J. Chem. Phys.*, 1983, **79**, 926-935.
- 64 P. E. M. Lopes, V. Murashov, M. Tazi, E. Demchuk and A. D. MacKerell, *J. Phys. Chem. B*, 2006, **110**, 2782-2792.
- 65 S. E. Feller, Y. Zhang, R. W. Pastor and B. R. Brooks, *J. Chem. Phys.*, 1995, **103**, 4613-4621.
- 66 J. P. Ryckaert, G. Ciccotti and H. J. C. Berendsen, *J. Comput. Phys.*, 1977, **23**, 327-341.
- 67 H. C. Andersen, *J. Comput. Phys.*, 1983, **52**, 24-34.
- 68 T. Darden, D. York and L. Pedersen, *J. Chem. Phys.*, 1993, **98**, 10089-10092.
- 69 M. E. Tuckerman, B. J. Berne and G. J. Martyna, *J. Chem. Phys.*, 1992, **97**, 1990-2001.

- 70 W. Humphrey, A. Dalke and K. Schulten, *J. Mol. Graphics*, 1996, **14**, 33-38.
- 71 E. R. Cruz-Chu, A. Aksimentiev and K. Schulten, *J. Phys. Chem. B*, 2006, **110**, 21497-21508.
- 72 R. Konecny, *iAPBS Interface on the Web*. <http://mccammon.ucsd.edu/iapbs> (accessed February 14, 2013).
- 73 P. A. Kollman, I. Massova, C. Reyes, B. Kuhn, S. H. Huo, L. Chong, M. Lee, T. Lee, Y. Duan, W. Wang, O. Donini, P. Cieplak, J. Srinivasan, D. A. Case and T. E. Cheatham, *Acc. Chem. Res.*, 2000, **33**, 889–897.
- 74 N. A. Baker, D. Sept, S. Joseph, M. J. Holst and J. A. McCammon, *Proc. Natl. Acad. Sci. U.S.A.*, 2001, **98**, 10037–10041.

TOC Graphic



Immobilization mode, microscopic structure and adsorption mechanism of papain on nanoporous silica surface